Combustion and Flame 188 (2018) 150–161

Contents lists available at ScienceDirect

Combustion and Flame

journal homepage: www.elsevier.com/locate/combustflame

A rapid compression machine study of autoignition, spark-ignition and flame propagation characteristics of $H_2/CH_4/CO$/air mixtures

Changpeng Liu[a], Heping Song[a], Peng Zhang[b], Zhi Wang[a,*], Margaret S Wooldridge[c,*], Xin He[d], Guotao Suo[e]

[a] State Key Laboratory of Automotive Safety and Energy, Tsinghua University, Automobile Research Institute, Room 112, Beijing 100084, China
[b] Center for Combustion Energy, Tsinghua University, Beijing 100084, China
[c] Departments of Mechanical and Aerospace Engineering, University of Michigan, 3546 George G. Brown Laboratory, 2350 Hayward, Ann Arbor, MI 48109, USA
[d] Aramco Services Company, Aramco Research Center – Detroit, Novi, MI 48377, USA
[e] Cummins (China) Investment Co., Ltd, Beijing 100004, China

ARTICLE INFO

Article history:
Received 4 January 2017
Revised 6 March 2017
Accepted 21 September 2017
Available online 17 October 2017

Keywords:
Natural gas
Dedicated-EGR
Hydrogen
Ignition delay time
Flame speed
Rapid compression machine

ABSTRACT

Recent years have seen increased interest in dedicated exhaust gas recirculation (D-EGR) systems integrated with reciprocating engines. By dedicating one cylinder to operate at fuel rich conditions, hydrogen is generated for use in the remaining cylinders to optimize combustion and mitigate pollutant emissions. In this study, experiments were performed using a rapid compression machine (RCM) to investigate the effects of hydrogen and carbon monoxide on methane ignition and flame propagation at fuel rich and stoichiometric conditions relevant to D-EGR engines. The experiments were conducted over a range of temperatures ($T = 860–1080$ K) and equivalence ratios ($\phi = 1.0–1.5$) and at a pressure of $P = 20$ atm. The results showed hydrogen addition had little effect on ignition delay time at lower temperatures ($T <$ 950 K), but hydrogen significantly promoted ignition at higher temperatures ($T >$ 950 K). Carbon monoxide had little effect on ignition delay times at all conditions studied. Combustion products were acquired using a fast sampling system and analyzed using gas chromatography. The results showed at $\phi = 1.4$ the hydrogen mole fraction was a maximum of 8.0% of the products of rich combustion which was consistent with predictions based on chemical equilibrium calculations and model simulation results. High speed images were taken to quantify the impact of equivalence ratio on flame speed for spark-ignited mixtures in RCM experiments using mixtures similar to those expected in the D-EGR and stoichiometric cylinders. The results indicated the H_2 in the D-EGR promoted the combustion process in the stoichiometric cylinder, increasing flame speed and decreasing combustion duration. Specifically, when the equivalence ratio in the D-EGR cylinder was $\phi = 1.3$, the flame speed increased by about 40% compared with $\phi = 1.0$. However, higher equivalence ratios reduced the flame speed and thus adversely affected combustion in the D-EGR cylinder. The results indicate stability and effectiveness of the combustion in the D-EGR cylinder could be a major concern for D-EGR natural gas engines, and optimizing the equivalence ratio of the D-EGR cylinder is critical for D-EGR to enhance combustion performance in the engine overall.

© 2017 The Combustion Institute. Published by Elsevier Inc. All rights reserved.

1. Introduction

Natural gas is a promising fuel for reciprocating internal combustion (IC) engines because of its low cost, high H/C ratio, and lower criteria pollutant emissions [1–3]. To meet stringent EPA and Euro VI emissions regulations, most state-of-the-art natural gas engines are designed to operate at stoichiometric conditions so the three-way catalyst (TWC) can be used to reduce tail-pipe pollutant emissions. Spark ignited natural gas engines can be designed with higher compression ratios (CR~12) than conventional gasoline engines due to the higher octane rating of natural gas. However, natural gas occupies a larger volume in the cylinder as a gaseous fuel which causes lower volumetric efficiency, reducing engine power density [4].

For spark-ignition, natural gas engines, engine knock and high thermal load are the two major constraints limiting engine compression ratio. Exhaust gas recirculation (EGR) is an effective way to reduce combustion temperatures so simultaneous reduction in

* Corresponding authors.
E-mail addresses: wangzhi@tsinghua.edu.cn (Z. Wang), mswool@umich.edu (M.S. Wooldridge).

https://doi.org/10.1016/j.combustflame.2017.09.031
0010-2180/© 2017 The Combustion Institute. Published by Elsevier Inc. All rights reserved.

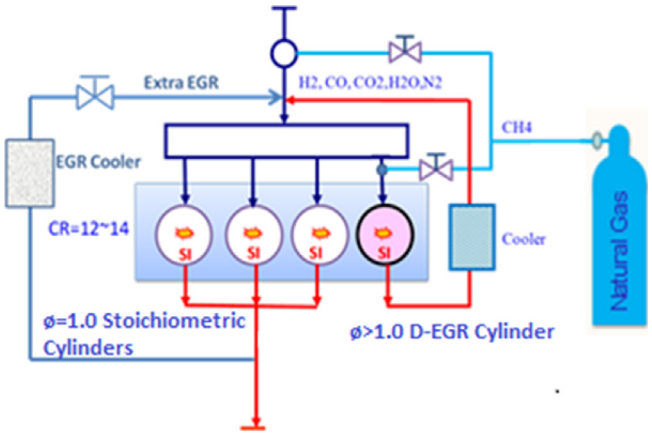

Fig. 1. Schematic of a spark ignited D-EGR natural gas IC engine.

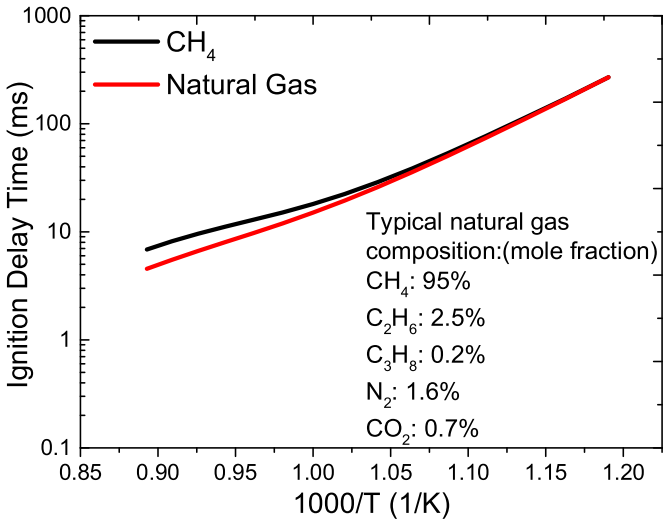

Fig. 2. Comparison of ignition delay times of CH_4 and a simulated natural gas mixture using the ARAMCOMECH 2.0 mechanism [52] for $P = 20$ atm.

NO_x emissions and thermal load can be achieved. However, EGR decreases flame speed, which deteriorates combustion stability and engine efficiency [5]. When natural gas is used in real IC engines, more and more studies are focusing on hydrogen enriched natural gas combustion as a means to increase flame speeds and improve volumetric efficiency [6–8]. Many studies have been conducted to measure the laminar flame speed of methane (the primary component of natural gas) at various temperatures and pressures [9–13]. Studies have found hydrogen can exponentially increase the flame speed of stoichiometric methane/air mixtures with increasing hydrogen fraction [14–20]. For IC engines, hydrogen addition has two additional significant benefits: reducing cycle-to-cycle variations at fuel lean operating conditions and increasing EGR tolerance [21–24].

Considering the difficulties of incorporating a hydrogen fueling system in addition to the main fueling system in real engines, a concept of dedicated EGR (D-EGR) has been proposed for onboard hydrogen generation [25]. Taking a four-cylinder IC engine as an example, one of the four cylinders operates at fuel rich conditions to produce hydrogen and carbon monoxide. All the exhaust gases from the D-EGR cylinder are circulated back into the intake manifold where the gases are inducted into the other three cylinders which operate at stoichiometric or fuel lean conditions. Figure 1 shows a schematic of a spark ignited D-EGR natural gas engine. Southwest Research Institute (SwRI) has studied D-EGR performance in gasoline and diesel engines. The results show D-EGR improved gasoline engine thermal efficiency by at least 10% [25,26]. Recently, Lee et al. [27] studied the potential of D-EGR in SI engines fueled by natural gas using computational fluid dynamics (CFD) simulations. The simulations predicted D-EGR is able to achieve thermal efficiencies similar to conventional SI engines while simultaneously reducing NO_x emissions.

In order to better understand natural gas and hydrogen combustion in real engines, the autoignition characteristics of methane and hydrogen mixtures, which control end-gas knock, should be well understood. Numerous studies, including experiments and numerical simulations, have been conducted to develop methane oxidation mechanisms. Ignition delay times of methane have been measured in many studies for a large range of mixtures and state conditions using rapid compression machines (RCMs) [28–37] (pressures and temperatures in the ranges of 16–40 atm and 920–1040 K) and shock tubes [29,34,36,38,39] (pressures and temperatures in the ranges of 10–260 atm and 1000–1550 K). Petersen et al. [29] studied methane ignition at conditions relevant to D-EGR. They measured ignition delay in low-dilution methane/air mixtures at high pressures (40–260 atm) and high temperatures (1040–1500 K) and developed a kinetic model based on the GRI-MECH 1.2 mechanism [40]. Goy et al. [28] studied the autoignition characteristics of methane at conditions relevant to gas turbines using an RCM. They concluded GRI-MECH overpredicted the ignition delay time for methane in the low temperature region ($T < 1250$ K). In the intermediate and low temperature regions ($T = 950$ K–1200 K), discrepancies were observed between experimental results and mechanism predictions for methane, especially at conditions relevant to spark-ignition engines (900 K, 20 atm). Recently, significant progress has been made in predicting methane ignition delay times with revised reaction mechanisms. More experimental data of methane/hydrogen/carbon monoxide/air mixtures, particularly rich fuel/air mixtures at high pressure and in the intermediate and low temperature region are valuable to quantify the effects of fuel rich conditions of hydrogen on methane ignition and to validate our predictive understanding of the methane/hydrogen/carbon monoxide/air combustion mechanism. This work focuses on low temperature ($T < 1100$ K), stoichiometric and fuel rich mixtures of methane, methane/hydrogen and methane/hydrogen/carbon monoxide fuel mixtures at moderate to high pressures ($P > 15$ atm).

The composition of natural gas varies depending on the source and the processing; however, methane is typically 95% (mole fraction basis) of the natural gas mixture. Generally, natural gas also includes small fractions of ethane, propane, nitrogen and carbon dioxide. Methane is often used as a surrogate for natural gas, particularly for ignition studies, as methane ignition is very consistent with natural gas ignition. For example, Fig. 2 compares predicted ignition delay times for methane and for a mixture of gases representative of typical natural gas composition [41]. The predictions were made using the ARAMCO [42] reaction mechanism for stoichiometric fuel/air mixtures for a pressure of 20 atm at air levels of dilution. At temperatures below 950 K, there is negligible difference between the model predictions. In the current study, to simplify the experimental process, pure methane was chosen as the surrogate of natural gas.

The presence of hydrogen in methane/air mixtures has a significant effect on the ignition process. Gersen et al. [31] studied combustion behavior of methane/hydrogen mixtures under stoichiometric conditions at temperatures between 950 and 1060 K, and pressures between 15 and 70 atm using an RCM. Hydrogen/methane mixtures, $5\%H_2/95\%CH_4$, $10\%H_2/90\%CH_4$, $20\%H_2/80\%CH_4$, and $50\%H_2/50\%CH_4$, were tested, and the ratio of total inert gases to oxidizer was close to that of nitrogen to

oxygen in air. They found hydrogen decreased the ignition delay time of methane at all conditions studied. They developed the following correlation to predict the ignition delay time of methane and hydrogen mixtures:

$$\tau = A_{H_2}^{\beta} \cdot A_{CH_4}^{(1-\beta)} \left(\frac{P_c}{T_c}\right)^{n_{H_2}^{\beta} + n_{CH_4}^{(1-\beta)}} \exp\left(\frac{E_{H_2}\ \beta + E_{CH_4}(1-\beta)}{RT}\right) \quad (1)$$

where P_c and T_c are pressure and temperature at the end of compression, R is the gas constant, β is the mole fraction of hydrogen in the fuel, and A, E, n are the fit coefficients for pure methane and pure hydrogen; their values can be found in [31]. The correlation shows the strong sensitivity of ignition delay time to the amount of H_2 in the fuel mixture. Similarly, Huang et al. [38,43], Zhang et al. [44,45], and Donohoe et al. [46] also studied the combustion characteristics and reaction kinetics of methane/hydrogen mixtures at intermediate and low temperatures (T = 850–1800 K).

In D-EGR combustion, carbon monoxide is also a main component of the exhaust gas of the rich cylinder. Gersen et al. [32] studied the effects of carbon monoxide addition on the autoignition of CH_4 and CH_4/H_2 fuels at high pressure in an RCM, and found CO had little effect on ignition delay times of CH_4 and CH_4/H_2 fuels at pressures ranging from 20 to 80 atm and in the temperature range 900–1100 K. Yu et al. [33] also found CO had no discernible effect on the ignition delay times of natural gas when CO proportions ranged from 10% to 30% in the reactant mixture and the equivalence ratio was held constant at $\phi = 1.0$. In summary, several experimental and numerical investigations have demonstrated hydrogen addition promotes methane ignition. However, discrepancies between experimental data and model predictions still exist at low temperatures (T < 1100 K).

Many experiments to understand and improve combustion characteristics of hydrogen, methane, and air have been performed using IC engines. Since fuel lean combustion is an effective way to increase efficiency and reduce NO_x emissions, some studies focused on extending the lean limit of natural gas fueled engines by adding hydrogen. Mariani et al. [47] compared natural gas and hydrogen-natural gas blends using a spark ignition engine. They found 30% (volume basis) hydrogen blended with 70% compressed natural gas decreased the combustion duration by 16%, reduced CO_2 emissions by 7%, and improved cycle-to-cycle variation particularly at low loads. Ma et al. [48], Bysveen [49], and Huang and coworkers [50] confirmed hydrogen addition extended the lean limit and increased engine power density. Saanum et al. [51] compared engine performance operating at lean and stoichiometric conditions with EGR and a TWC. The results showed with 25% hydrogen addition, lean conditions exhibited much higher NO_x emissions than stoichiometric conditions with EGR and TWC.

In real engine applications, on-board hydrogen generation is preferred to minimize system costs. In-cylinder methane reforming could be an effective way to produce hydrogen on-demand in an engine. Thus, the objective of this study was to quantify the autoignition, spark ignition and flame propagation characteristics of stoichiometric and fuel rich hydrogen, methane, carbon monoxide and air mixtures in the context of developing D-EGR natural gas engines. The approach was to measure the ignition delay time and product species of hydrogen, methane and air mixtures at conditions important to D-EGR natural gas fueled engines using an RCM. The results were used to determine realistic concentrations of hydrogen and other exhaust gases that can be produced in a D-EGR cylinder. The RCM was then equipped with a spark ignition system to study ignition and flame propagation of mixtures representative of engine cylinders using the D-EGR product gases. The results are discussed in terms of optimizing D-EGR for natural gas engines.

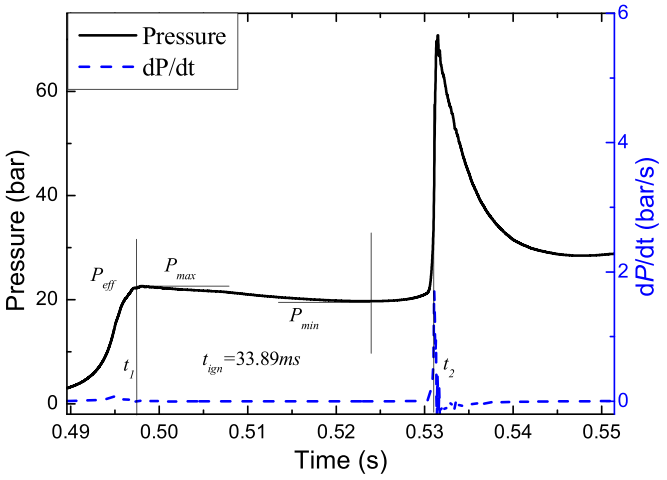

Fig. 3. Typical pressure data of methane autoignition, including an illustration of the method used to determine the effective pressure and the ignition delay time for each experiment. (For interpretation of the references to color in this figure, the reader is referred to the web version of this article).

2. Experimental and computational methods

2.1. The rapid compression machine

All experiments were conducted using an RCM at Tsinghua University (TU). A detailed description of the TU RCM with fast sampling and optical diagnostics can be found in Di et al. [52] and Wang et al. [53]. Briefly, the RCM consists of five major components: the high pressure air tank, the driver section, the hydraulic section, the driven section and the test section. The components are aligned and connected by two rods. The air tank supplies the driving power to push the pistons forward. The driven section has a length of 0.5 m and 50.8 mm inner diameter. In order to achieve different temperatures, the test section consists of components that permit control of the overall length of the test section, which can be varied from 13 mm to 80 mm. Changing the length of the test section changes the compression ratio of the RCM, and thereby makes changing the end-of-compression temperature and pressure straightforward. The compression process of the TU RCM takes about 25–30 ms, which elevates the mixture to the desired high pressure and high temperature condition. A creviced piston design was used to reduce the effects of cooler gases in the boundary layer entering the test section during the compression process. The pressure traces were obtained using a piezoelectric transducer (Kistler 6125C) in the test section. For the current study, the experiments were conducted at an end of compression (EOC) pressure of about 20 atm and EOC temperatures in the range of 860 to 1080 K.

Figure 3 presents typical pressure data of a methane TU RCM ignition experiment. The black line is the pressure in the test section, while the blue dotted line is the first derivative of the pressure data. Time t = 0 s corresponds to the first local peak pressure due to compression. For each experiment, the state condition was defined using the same method presented in [50]. First, an effective pressure (P_{eff}) was defined as

$$P_{eff} = \frac{1}{(t_2 - t_1)} \int_{t_1}^{t_2} P dt \quad (2)$$

where t_1 was the time of peak pressure due to compression, and t_2 was the time of local minimum pressure (due to cooling) after compression, but before ignition. The effective temperature (T_{eff})

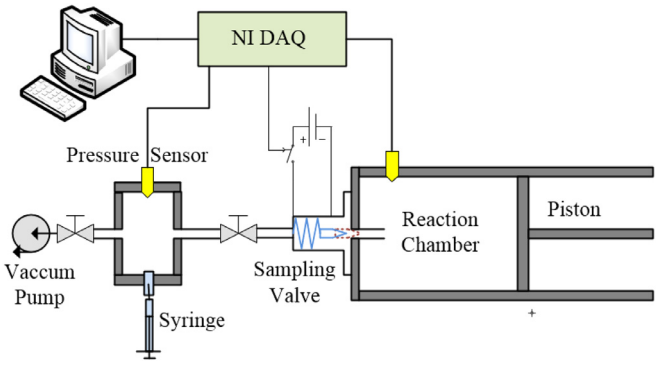

Fig. 4. Schematic of the fast gas sampling system.

was calculated using P_{eff} and the initial pressure P_0:

$$\int_{T_0}^{T_{eff}} \frac{\gamma}{\gamma - 1} d\ln T = \ln\left(\frac{P_{eff}}{P_0}\right) \tag{3}$$

where γ was the temperature dependent ratio of the specific heats of the test mixture. The ignition delay time, τ_{ign}, for each experiment was defined as the time from the end of compression to time of maximum dP/dt due to ignition, $\tau_{ign} = t_{dP/dt,max} - t_0$, as shown in Fig. 3.

For some experiments, a spark ignition system was used to initiate a flame after the EOC. The EOC conditions were used to define the state conditions for the spark ignition experiments. For the spark ignition experiments, the RCM was equipped with a quartz window at the end wall, which allowed visualization of the test section along the axial direction. Using a high-speed camera (Photron Fastcam SAX2, model 1000 K) with a Nikon 50 mm lens, color images were recorded at 20,000 frames per second with a CMOS array resolution of 512 × 512 pixels. The location of the flame front was determined from the images, and image processing was used to determine the flame propagation rates as a function of time for each imaging experiment.

2.2. Gas sampling and gas chromatography

A fast sampling system was used to acquire gas samples of the combustion products. A detailed description of the fast sampling system can be found in [54]. Briefly, the fast sampling system consisted of a sampling probe, a fast-acting solenoid valve, a vacuum pump, and a sample tank, with a volume of approximately 5.4 mL. Figure 4 is a schematic of the fast sampling system. The sample tank was equipped with a piezoresistive pressure transducer (Kistler 4045A5) and amplifier (Kistler 4618A0) and a septum port for gas extraction. The sampling probe (1 mm in inner diameter) was installed on the RCM end wall. The open end of the probe was located at the center of the test section, 5 mm from the end wall.

The sampled gases were removed by syringe from the sampling volume and were injected into a gas chromatograph (Agilent 7890B) for analysis. Gas chromatography (GC) was used to quantify the concentrations of the stable species in the combustion products. A flame ionization detector was used to measure CH_4 and H_2 concentrations and a thermal conductivity detector was used to measure CO and CO_2 concentrations. The detailed GC configuration, measured species and corresponding retention times are provided in the Supplementary Material. Ultra-high purity helium (Beijing Hua Yuan Gas, Purity Plus, 99.999%) was used as the carrier gas for all experiments. Standard calibration mixtures of CH_4, H_2, CO, CO_2 and N_2 (Beijing Hua Yuan Gas) were prepared using the RCM mixing tank and gas manifold and the mixtures were used for the GC calibration. Signals from the GC detectors were recorded and analyzed using Agilent Open LAB software. The ratio of peak area to mole fraction was used to determine the calibration factors. Gas sampling and GC analysis were not used with the spark ignition study.

The primary sources of uncertainty in the fast sampling measurements were due to the dilution of the unreacted gases trapped in the 'dead' volume, which was defined as the total volume in the sampling probe and the fast sampling valve exposed to the reactant gases, estimated as 0.017 mL. The species mole fractions in the core region, χ_{core}, were corrected using the following equation [54].

$$\chi_{core} = \frac{\chi_{sampling}}{1 - \xi} \tag{4}$$

where $\chi_{sampling}$ is the species mole fraction in the sample tank determined using the GC measurement, and ξ is the dilution ratio, which was calculated using the following relation.

$$\xi = \frac{P_{chamber} \cdot V_{dead}}{T_{dead}} \frac{T_{sampling}}{P_{sampling} \cdot V_{sampling}} \tag{5}$$

In Eq. (5), $P_{chamber}$ is the average combustion chamber pressure during the sampling time, T_{dead} is the average temperature in the dead volume, $P_{sampling}$ is the final pressure in the sample tank, $V_{sampling}$ is the total volume of the sample tank, and $T_{sampling}$ is the final gas temperature in the sample tank, which was room temperature in the current study. The gas temperature in the dead volume (T_{dead}) was not directly measured and was the major source of the uncertainty in determining the dilution ratio. The lower and upper limits of T_{dead} were the initial gas temperature (~25 °C) and the core gas temperature in the combustion chamber during sampling. Based on the experimental conditions of the sampling experiments, the dilution ratio was 0.8–3.15%. Another source of uncertainty was from the GC calibration, which was estimated as 4% of the species concentration. All sampling experiments were repeated at least three times. The total measurement uncertainty in the current study was calculated by assuming independent contributions from the GC calibration uncertainty, the "dead volume" uncertainty, and the standard deviation of the experiments.

2.3. Test mixtures

Test mixtures were prepared in a stainless steel mixing tank. The mixture composition was determined using the partial pressures of the mixture components, which were measured using a pressure transducer (Omega DPG4000-15C-DC). Ultra-high purity grade argon (>99.999%), oxygen (>99.995%), methane (>99.999%), hydrogen (>99.999%), carbon dioxide (>99.999%) and carbon monoxide (>99.999%) were used. In this study, argon was used as dilution gas to achieve the desired EOC temperatures. Carbon dioxide was used as a constituent of the simulated D-EGR gases. Hydrogen, methane and carbon monoxide were used as the simulated D-EGR fuels for the study.

All experiments were conducted using either stoichiometric equivalence ratios ($\phi = 1.0$) or fuel rich conditions ($\phi > 1.0$). As noted earlier, the EOC pressure was kept constant at about 20 atm, which was controlled by adjusting the initial pressure of the test gas mixture. A range of effective temperatures was tested by changing the test section length.

2.4. Computational methods

Computational simulations were conducted using the CHEMKIN suite of software (CHEMKIN-PRO x32) [55] and assuming a closed 0-D homogenous batch reactor. The ARAMCOMECH 2.0 [42] reaction mechanism was used with the CHEMKIN simulations. For the

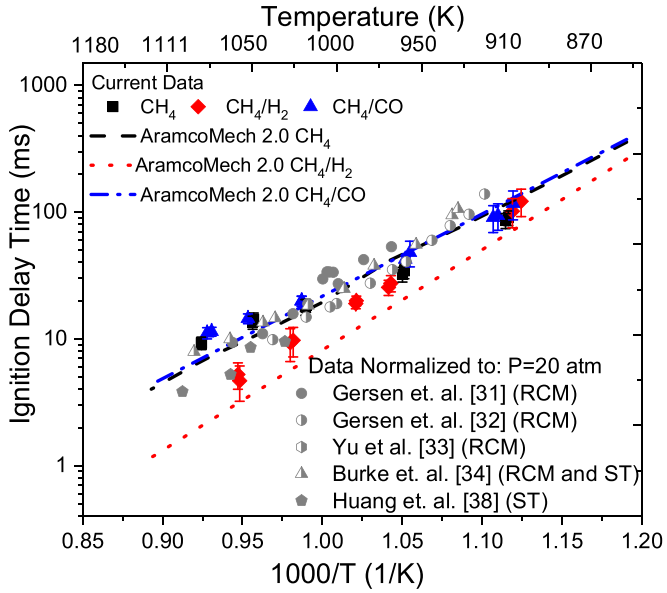

Fig. 5. Comparison of the effects of H_2 and CO addition on measured and predicted CH_4 ignition delay times. Gray symbols are CH_4 ignition delay data from previous studies, which have been normalized to $P = 20$ atm. The conditions of the simulation were $P_{eff} = 20$ atm, 100% CH_4 and 80% CH_4 and 20% H_2 (CO) and $\phi = 1$. The error bars are the uncertainties in the experimental measurements which are primarily due to the pressure and temperature measurements [52,54].

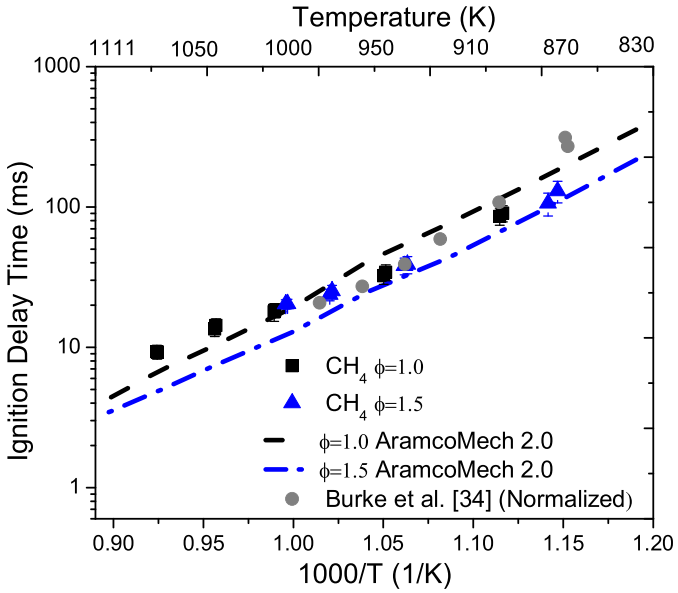

Fig. 6. Comparison of the effects of fuel-to-air equivalence ratio on measured and predicted CH_4 ignition delay times for $P = 20$ atm. Gray symbols are CH_4 ignition delay data ($\phi > 1.0$) from previous studies.

ignition delay time simulations, a variable volume model was used which included the compression and heat loss processes. The volume time history is provided in the Supplementary material and was obtained in the same manner as described in [56]. Sensitivity analysis at two temperatures (880 K and 1080 K) was performed to identify and compare the most important reactions to autoignition delay time between pure methane and methane/hydrogen blends.

The program BOOST (AVL) was used to simulate and calculate the concentrations of hydrogen and carbon monoxide in the intake manifold while running an engine model using a D-EGR mode of operation. The simulation model, which consisted of a series of elements that represented engine components, and the engine specifications used in the BOOST simulation are provided in the Supplementary Material. Each element of the model used basic equations to calculate values of various thermodynamic variables. Gas properties in the elements were calculated at each time step with instantaneous composition using solutions of gas dynamic equations [57]. For the BOOST simulations, the equivalence ratio in the D-cylinder was changed from 1.0 to 1.5 in increments of 0.1, while the equivalence ratios in the stoichiometric cylinders were kept at a constant value of $\phi = 1.0$. The intake composition data of the stoichiometric cylinders and the D-cylinder were recorded for each condition in the D-cylinder. Based on the results of the BOOST simulations, further RCM experiments were conducted to investigate the stoichiometric and D-cylinder combustion in the D-EGR mode.

3. Results and discussion

3.1. Ignition delay times

Ignition delay times of stoichiometric CH_4/air, CH_4/H_2/air, and CH_4/CO/air mixtures were measured to investigate the effects of H_2 and CO addition on CH_4 ignition. A table of the results is provided in the Supplementary Material. Figure 5 compares the experimental data with predictions using the ARAMCOMECH 2.0 [42] reaction mechanism. The experimental results show carbon monoxide (when included at 20% mole fraction of fuel) did not significantly affect the methane ignition delay time at any of the temperatures studied. At low temperatures ($T < 950$ K), hydrogen (when included at 20% mole fraction of fuel) did not significantly affect the methane ignition delay time either. However, hydrogen significantly promoted ignition at temperatures higher than 950 K, and the enhancement was more pronounced as temperature increased. The ARAMCOMECH 2.0 mechanism showed exceptional performance at reproducing the ignition delay time at all conditions and for all mixtures. The results of the current work are also compared with previous studies of CH_4/air ignition in Fig. 5. The data from the previous studies included in Fig. 5 were all obtained at stoichiometric conditions (without H_2 addition), and the inert:O_2 level was the same as the current experiments, specifically a molar ratio of 3.76:1. Since the previous studies span a range of pressures (15–40 atm), the data were normalized to the conditions of the current work ($P = 20$ atm) using the ARAMCO mechanism predictions for pressure dependence. Specifically, the ARAMCO mechanism predicts ignition delay time should scale as $\tau \propto P^{-1.36}$. The results of the current work are in excellent agreement with the previous experimental ignition studies.

Figure 6 compares the measured and predicted ignition delay times at different equivalence ratios ($\phi = 1.0$ and $\phi = 1.5$). No significant difference in ignition delay was observed in the experimental data between stoichiometric and fuel rich mixtures. The ARAMCO mechanism, however, predicted slightly faster (by ~20%) ignition delay times at fuel rich conditions, which is likely within the uncertainty of the model predictions. The experimental results of the current work are also compared with the results of the ignition study by Burke et al. [34] were scaled to the conditions of $P = 20$ atm and $\phi = 1.5$ using the ARAMCO mechanism predictions for dependence on pressure and equivalence ratio, where $\tau \propto P^{-1.36}\phi^{-0.25}$. The results of the current work are in excellent agreement with the previous experimental studies.

3.2. Fast sampling results

Gas chromatography was used to quantify the combustion products for the fuel rich ignition experiments as a function of equivalence ratio. Samples of the gases in the test section were acquired by opening a fast-acting solenoid valve between the test

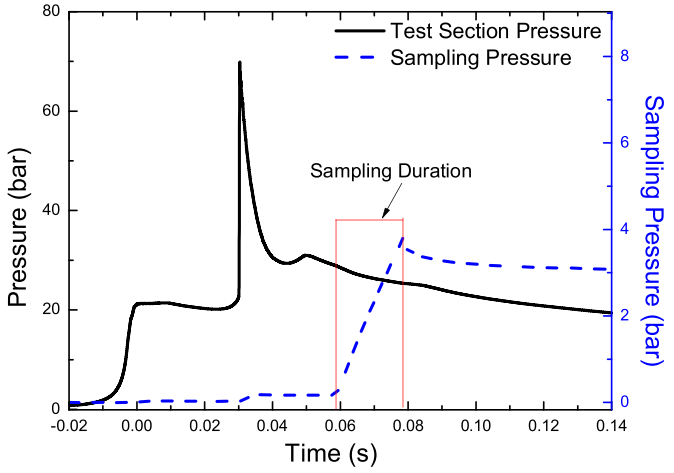

Fig. 7. Test section pressure and sampling pressure during the sampling process of a typical fuel rich ignition experiment. The conditions of the experiment were T_{eff} = 950 K, P_{eff} = 20 atm, CH_4 = 100%, and $\phi = 1.3$.

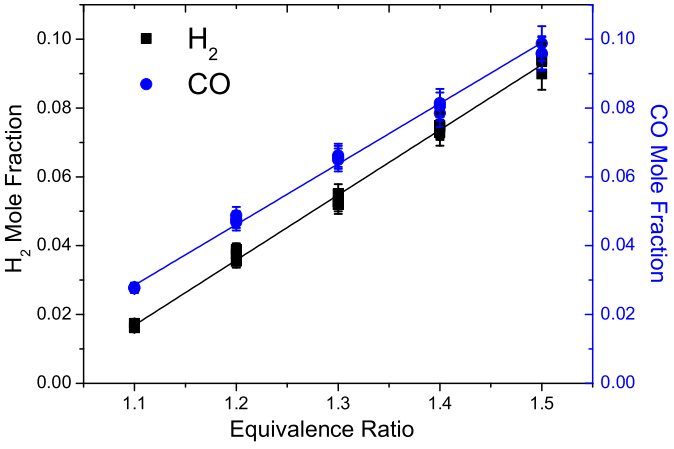

Fig. 8. Experimental results of the measurements of H_2 and CO in the combustion products of the fuel rich CH_4 ignition experiments.

section and an evacuated sampling chamber. In this study, a small amount (about 0.003%, volume basis) of the test gas mixture was withdrawn from the center of the test section after ignition, and the samples were used to determine the mole fractions of hydrogen and carbon monoxide in the combustion product of the experiments with $\phi = 1.1$ to $\phi = 1.5$.

Typical pressure time histories from the test section and the sampling chamber are shown in Fig. 7. After combustion, the high pressure in the test section pushed the piston away from the end

Table 1
Mixture compositions before combustion for different D-EGR equivalence ratios.

	D-EGR cylinder ϕ	Mole fraction %					
		CH_4	H_2	CO	O_2	CO_2	N_2
Stoichiometric cylinders	1.0	6.74	0	0	13.5	8.1	71.6
	1.1	6.55	0.28	0.32	13.33	8.11	71.4
	1.2	6.05	0.63	0.69	13.21	8.09	71.3
	1.3	5.81	1.08	1.09	13.08	7.94	71.0
	1.4	5.73	1.56	1.41	13.17	7.3	70.6
	1.5	5.65	2.14	1.78	13.18	7.04	70.2
D-EGR cylinder	1.0	6.74	0	0	13.5	8.1	71.6
	1.1	7.30	0.31	0.38	13.19	8.06	70.8
	1.2	7.66	0.69	0.77	13.0	7.91	70.0
	1.3	8.12	1.17	1.20	12.77	7.61	69.1
	1.4	9.09	1.72	1.56	12.71	7.0	67.9
	1.5	9.66	2.33	2.10	12.52	6.64	66.9

Table 2
RCM experimental conditions.

Parameter	Value
Effective compression ratio	10.6
Equivalence ratio	1.0–1.5
EOC temperature	~690 K
EOC pressure	~20 atm
Diameter of optical window	50.8 mm
Spark plug location	Center of the test section

wall, which caused a rapid decrease in pressure in the test section. (Note the piston movement after ignition had no effect on the measurement of the ignition delay time and combustion products because combustion completed before the piston movement.) The duration of the opening of the fast sampling valve, indicated by the red line in Fig. 7, was about 20 ms after ignition, to allow an adequate amount of the gas sample to be acquired. The pressure in the sampling chamber increased linearly during the sampling process and decreased slightly after valve closing due to cooling of the sample gas in the sampling chamber.

The results of the GC measurements are presented in Fig. 8. H_2 and CO increased with increasing equivalence ratio, and the molar ratio of H_2 to CO was close to 1.0 throughout the range of conditions studied. Approximately 8% mole fraction of H_2 was produced for $\phi = 1.4$, which translated to approximately 2% mole fraction of H_2 in the intake manifold for a four cylinder D-EGR engine, assuming the exhaust gases were well mixed with fresh air. The error bars are the experimental uncertainties described in Section 2.2.

The RCM results were compared with predictions for the product gas composition using AVL BOOST simulations, in order to verify the accuracy of the AVL BOOST model at predicting the combustion products. The experimental results were also compared with chemical equilibrium calculations assuming major products of

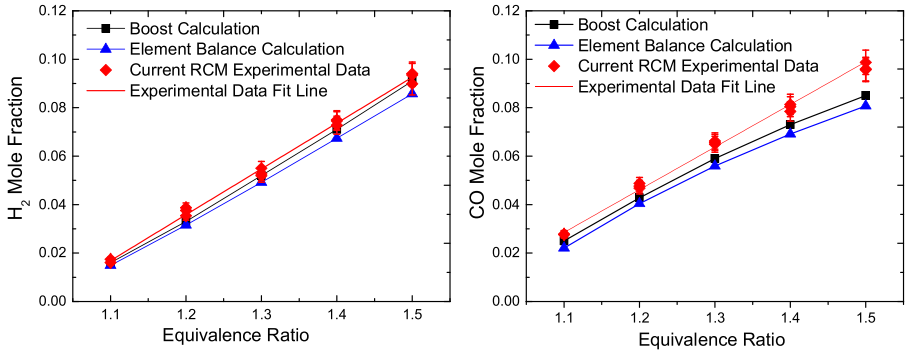

Fig. 9. Comparison of H_2 and CO measurements and calculations in the combustion products as a function of fuel rich conditions.

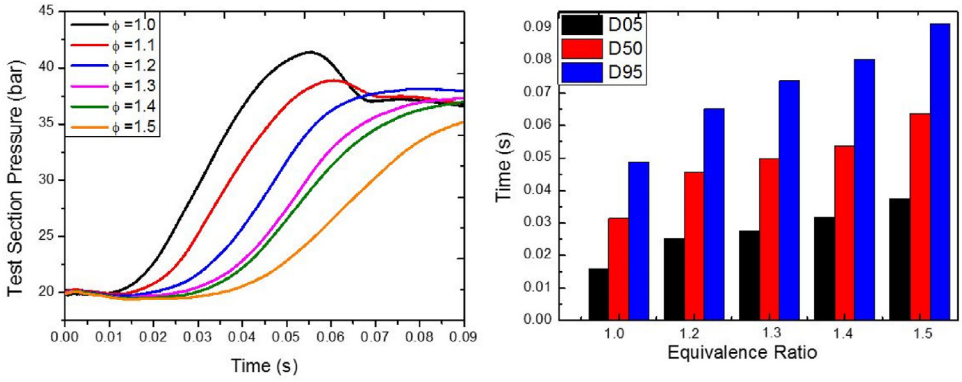

Fig. 10. Spark ignition results for test-section pressure (left panel) for the different D-EGR cylinder mixtures listed in Table 1. The right panel is the combustion duration corresponding to the pressure data.

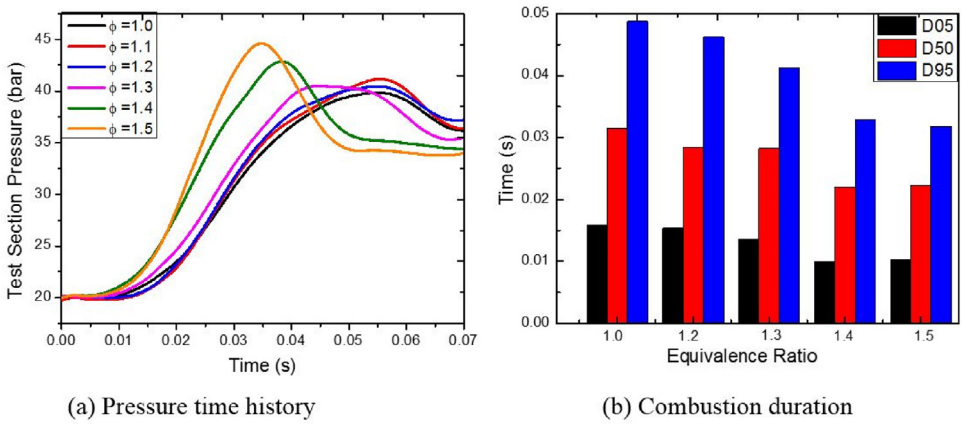

Fig. 11. Spark ignition results for the test section pressure (left panel) for the different stoichiometric cylinder mixtures listed in Table 1, where ϕ is the equivalence ratio in the D-EGR cylinder. The right panel is the combustion duration corresponding to the pressure data.

complete combustion. The global reaction for fuel rich combustion of methane can be written per mole of O_2 as [58]:

$$\varepsilon\phi C + 2(1-\varepsilon)\phi H_2 + O_2 + \delta N_2 = n_{CO_2}CO_2 + n_{H_2O}H_2O + n_{CO}CO + n_{H_2}H_2 + n_{O_2}O_2 + n_{N_2}N_2$$

where δ is the molar N_2/O_2 ratio (3.773 for air), $\varepsilon = 4/(4+y)$, y is the molar H/C ratio of the fuel, ϕ is fuel/air equivalence ratio, and n_i is number of moles of species i (where i = CO_2, H_2O, CO, H_2, O_2 or N_2) per mole of O_2 reactant. Because the focus was on fuel rich combustion, O_2 was neglected as a product of combustion. In addition to the element balance equations, the water–gas shift reaction $CO_2 + H_2 = CO + H_2O$ was used to provide closure for the equilibrium calculations, with the equilibrium constant K (T):

$$K(T) = \frac{n_{H_2O}n_{CO}}{n_{CO_2}n_{H_2}} \tag{7}$$

K (T) can be assumed constant over the normal engine operating range.

Figure 9 compares the H_2 and CO mole fractions measured in the fuel rich experiments with the results of the AVL BOOST simulations and the equilibrium calculations. The AVL BOOST results agreed well with the experimental data and the equilibrium calculations, where the modeling results for H_2 were within 8.0% of the experimental data, and the CO modeling results were within 13% of the experimental data. For the CO, the experimental data were systematically higher than the model predictions with higher differences at higher equivalence ratio. The comparison built confidence for using the AVL BOOST simulations to accurately predict the product compositions of natural gas D-EGR engines.

3.3. Dedicated EGR combustion

In the D-EGR mode, one cylinder operates at fuel rich conditions, and the other cylinders operate at stoichiometric or fuel lean conditions. Since the D-EGR cylinder can operate using a range of equivalence ratios with $\phi > 1.0$, it is important to understand what the effects are of the range of product gas compositions on the rest of the cylinders. In this part of the study, the AVL BOOST model (shown in the Supplementary Material) was used to calculate the in-cylinder mixture compositions, before combustion, of an I-4 methane-fueled D-EGR engine. The cylinder 4 is the D-EGR cylinder, operating at $\phi > 1.0$, and the other three cylinders operate at stoichiometric conditions. The concentrations of CH_4, H_2, CO, CO_2, O_2, N_2 and H_2O reported here were determined after the simulations had reached steady state conditions (after more than 100 simulation cycles).

Table 1 shows the predicted concentrations of the species CH_4, H_2, CO, CO_2, O_2, N_2 and H_2O, for the two categories of cylinders, i.e. the cylinders operated at $\phi = 1.0$ and the D-EGR cylinder operated at $\phi \geq 1.0$.

Based on the results, mixtures of $CH_4/H_2/CO/O_2/CO_2/N_2$ were prepared for further RCM experiments to understand the impact of the D-EGR equivalence ratio on the combustion processes in both D-EGR and stoichiometric cylinders. In the experiments, H_2O was replaced by CO_2 to eliminate potential condensation. At the

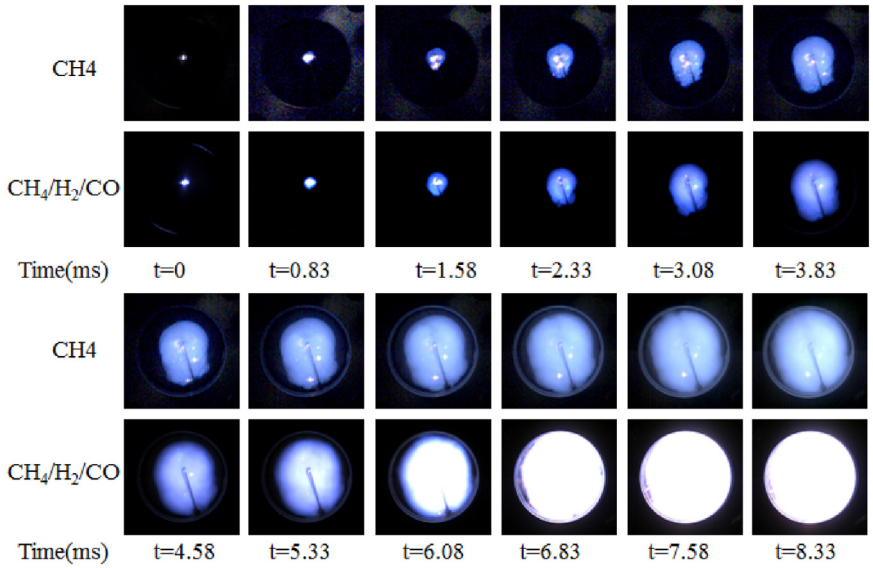

Fig. 12. Images from the digital video recordings of spark ignition experiments of CH_4 (top panels) and $CH_4/H_2/CO$ (bottom panels), both without EGR at $\phi = 1.0$, $P_{eff} = 20$ atm and $T_{EOC} = 690$ K.

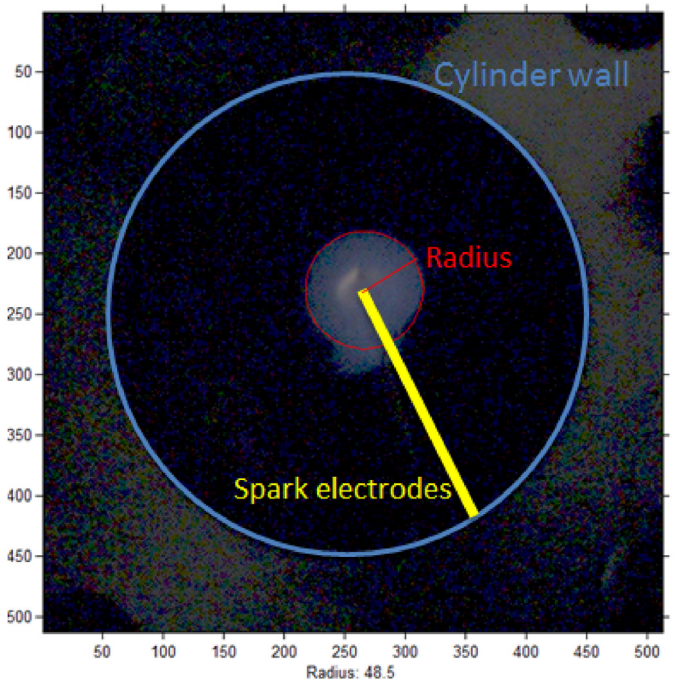

Fig. 13. Equivalent radius of flame front in directions unaffected by the spark electrodes.

temperature, pressure and mixtures studied, H_2O was not expected to have a significant chemical effect on the ignition process as was observed in the study by Donohoe et al. [30] on the effects of water addition to syngas and natural gas ignition delay times. Table 2 shows the experimental conditions of these spark ignited mixtures. All experiments were conducted using the same effective compression ratio of approximately 10.6 (similar to real spark ignition engines). A custom spark plug with electrodes located in the center of the test section was used to initiate combustion. The spark timing was controlled to 0.2 ms ± 0.05 ms after compression. All experiments targeted the same P_{eff} and EOC temperature, with small variations in state conditions based on the different heat capacities of the different test gas mixtures.

Figure 10 shows the results for the pressure time histories and the corresponding combustion durations at different equivalence ratios for the mixtures associated with the D-EGR cylinder. Time $t = 0$ ms represents the start of spark firing. The heat release rate, $\frac{dQ}{dt}$, for each experiment was calculated based on the pressure data and then used to quantify combustion duration:

$$\frac{dQ}{dt} = \left(\frac{1}{\gamma - 1} * V * \frac{dP}{dt}\right) \tag{8}$$

where V is the volume of test section and γ is the isentropic exponent and $\gamma = 1.35$. D05, D50, and D95 are the time intervals between the start of spark firing and 5%, 50%, and 95% of total heat release, respectively.

As seen in Fig. 10, the peak combustion pressure decreased and the combustion duration increased with increasing equivalence ratio. The results indicate the combustion process deteriorated as ϕ increased even with H_2 in the fuel/air mixture. D05, a key parameter representing the resistance to ignition of the mixture, also increased with increasing equivalence ratio. The results indicate H_2 addition in the D-EGR cylinder did not offset the negative impact of CH_4 enrichment.

Figure 11 shows the results for the pressure time histories and the corresponding combustion durations at different equivalence ratios for the mixtures associated with the stoichiometric cylinders (see Table 1 for the mixture compositions). With higher equivalence ratio in the D-EGR cylinder, more H_2 was produced, which promoted combustion in the stoichiometric cylinder mixtures. Compared with $\phi = 1.0$, the combustion duration decreased by about 35% when the equivalence ratio in the D-EGR cylinder was $\phi = 1.4$. The combined results of Figs. 10 and 11 demonstrate the challenge of optimizing the equivalence ratio in the D-EGR cylinder to maintain robust combustion while still enhancing combustion in the stoichiometric cylinder.

3.4. Flame speed

By replacing the end wall with a quartz optical window, the ignition and combustion processes were visualized in the axial direction using a high-speed camera. Based on the images, an effective flame speed was quantified. Figure 12 presents images from

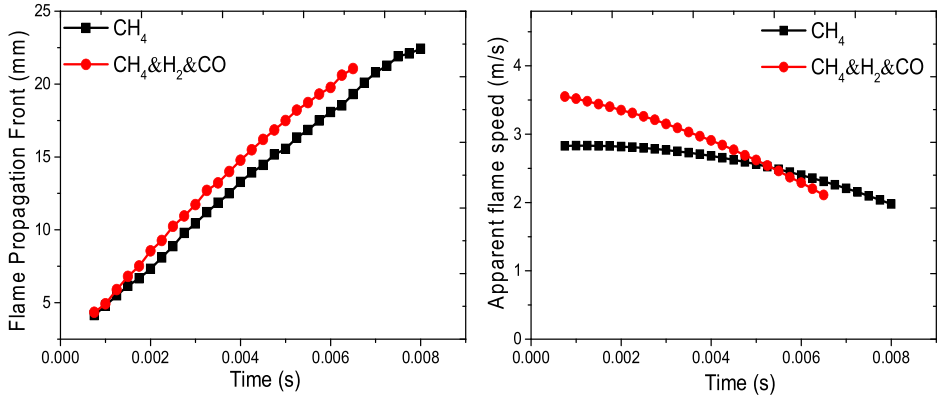

Fig. 14. Equivalent flame radius determined from the high speed imaging and corresponding flame speed of CH_4 and $CH_4/H_2/CO$ (2% H_2/CO) at $\phi = 1.0$.

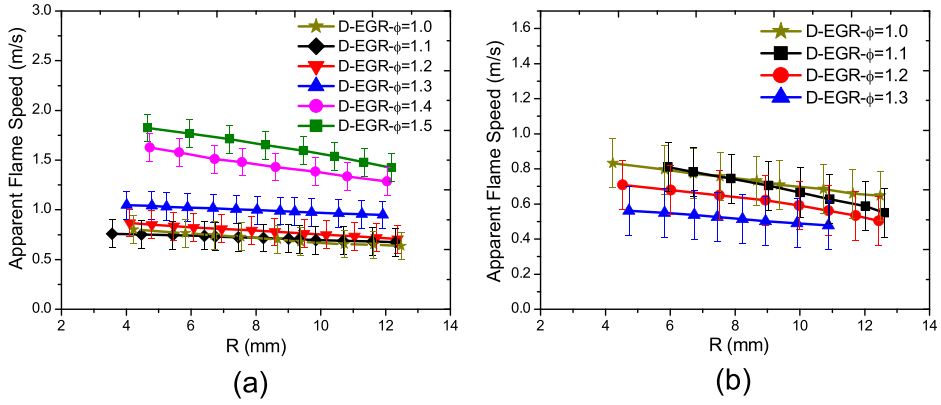

Fig. 15. Experimental results for the apparent flame speed as a function of flame radius and D-EGR equivalence ratio for (a) stoichiometric cylinder mixtures and (b) D-EGR cylinder mixtures. All experiments were conducted at $P_{eff} = 20$ atm and $T_{EOC} \cong 690$ K.

RCM experiments of CH_4 and a $CH_4/H_2/CO$ mixture (2% H_2 /CO, $H_2/CH_4 = 1/4$) at $\phi = 1.0$.

The images in Fig. 12 show the spark electrodes had apparent impact on the flame propagation, as the flame appeared to propagate faster along the electrodes. In this study, the apparent flame speed was calculated using

$$V = \frac{R_{t+1} - R_t}{\Delta t} \tag{9}$$

where Δt is the time interval between two images, R is the equivalent radius of the flame in the direction apparently unaffected by the spark electrodes, as shown in Fig. 13. The apparent flame speed data were not corrected for stretch, density changes, or the effects of the proximity of ignition energy of the spark charge. The propagation rate data describe the apparent or observed expansion rate of the flame surface. At the beginning of the flame propagation, the flame speed was significantly influenced by the spark electrodes and thus only images with flame radius larger than 4 mm were analyzed. Note, although the RCM was designed to minimize gas motion after compression, the flames were affected by changing density and heat losses. Thus, the flame speeds presented in this study are not fundamental laminar flame speeds. As with the D-EGR combustion duration experiments, the imaging experiments were all conducted with the same RCM configuration and operating conditions; the only difference between experiments was the mixture composition. Thus, the results approximately isolated the effects of mixture composition on flame propagation.

Figure 14 shows the evolution of the equivalent radius and apparent flame speed for a CH_4 and a $CH_4/H_2/CO$ mixture. The apparent flame speed decreased as the radius increased for both fuel compositions. This was attributed to the increasing pressure of the unburned mixture and heat losses as the flame approached the cold cylinder walls. Since the radius of the combustion chamber was 25.4 mm, the analysis focused on flame speeds derived when the flame radius was between 4 and 12.5 mm. When the flame radius reached 12.5 mm, the total pressure had increased by less than 2.0%. The mean flame propagation speeds of the two cases were 2.7 m/s for CH_4 and 3.3 m/s for $CH_4/H_2/CO$.

Figure 15 presents the effects of the D-EGR equivalence ratio on the apparent flame speed of the mixtures representative of the stoichiometric cylinder in the left panel and of the D-EGR cylinder in the right panel. The error bars are the experimental uncertainties. Two measurement uncertainties were considered: the uncertainty in processing the images (capturing the flame front positions) and the standard deviation of repeated experiments. The uncertainty in measuring the flame radius was the distance represented by one pixel, which was 0.12 mm. This translated to ± 0.12 m/s in apparent flame speed. The maximum standard deviation of repeated experiments was 0.08 m/s. Treating these as independent sources of error (i.e., taking the square root of the sum of the squares of the two uncertainties), the maximum measurement uncertainty was ± 0.14 m/s. The mixture compositions and experimental conditions were the same as presented in Tables 1 and 2. Increasing the D-EGR equivalence ratio promoted the combustion process in the stoichiometric cylinder mixtures, which was consistent with the observations based on the combustion duration calculated from the pressure data. The apparent flame speed was over a factor of two higher for the $\phi = 1.4$ and 1.5 cases compared with the $\phi = 1.0$ base case for the stoichiometric cylinder mixtures. As ϕ increased in the EGR mixture, the higher levels of hydrogen increased the

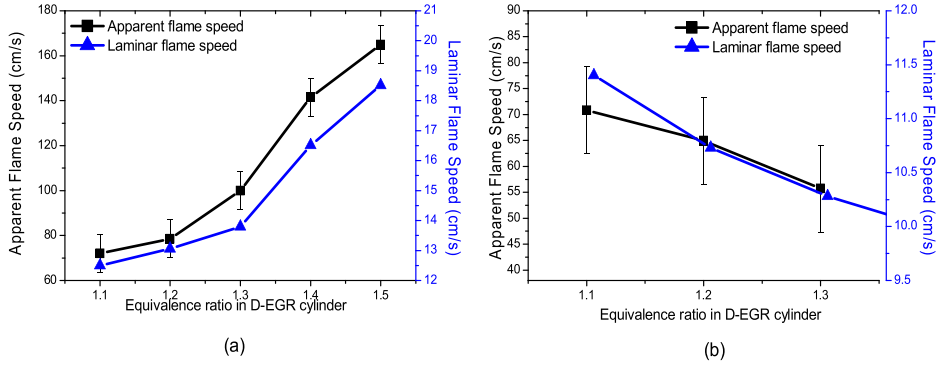

Fig. 16. Comparison of experimentally determined apparent flame speeds with simulation results for one-dimensional laminar flame speeds as a function of D-EGR equivalence ratio for (a) stoichiometric cylinder mixtures and (b) D-EGR cylinder mixtures. Experimental data were collected at $R = 8.0$ mm.

flame speeds for all the stoichiometric cylinder mixtures. The converse was true of the flames speeds observed in the D-EGR mixtures. As seen in Fig. 15, the richer mixtures exhibited slower flame speeds, decreased by about 20% when the equivalence ratio increased from 1.0 to 1.3. Although higher equivalence ratios generated more hydrogen, the results indicated the combustion process was predominately influenced by the equivalence ratio. Excess CH_4 suppressed flame propagation, resulting in lower flame speeds. Note for experiments with $\phi > 1.4$, the chemiluminescence intensities were too weak to clearly identify the flame front position and thus flame speed data could not be determined.

Figure 16 shows the chemical kinetic influence of D-EGR on CH_4 laminar flame speed, in comparison with the experimental results. The laminar flame speed was calculated using the CHEMKIN premixed laminar flame speed model. The simulation results for laminar flame speed exhibited the same trend as the measured apparent flame speeds. As the equivalence ratio in the D-EGR cylinder increased, more hydrogen in the mixture accelerated the laminar flame speed. For the D-EGR cylinder mixtures, the opposite behavior was observed due to the suppression of the flame speed due to the excess CH_4. The apparent flame speeds measured using the RCM were about 6–8 times faster than the simulation results for laminar flame speed, which is not surprising due to the differences between the RCM experiments and the simplified one-dimensional flame model, including turbulence, heat losses, and wall quenching effects.

4. Conclusions

The results of this study are the first combustion kinetic experiments to focus on conditions and mixtures important to the application of EGR to natural-gas fueled reciprocating engines. Although methane was used as a simple surrogate for natural gas and hydrogen and carbon monoxide mixtures were used as simple surrogates for EGR, the results provide insight into the benefits and challenges of using a cylinder for dedicated EGR while fueling the remaining cylinders at stoichiometric conditions. The major conclusions of the study are:

1. Ignition delay times of stoichiometric mixtures of CH_4, CH_4 and H_2, and CH_4 and CO were measured at temperatures ranging from 860 to 1080 K and a pressure at 20 atm. Hydrogen promoted CH_4 ignition at temperatures higher than 950 K, and the effects were more pronounced as temperature increased. Hydrogen addition had little effect on CH_4 ignition at lower temperatures ($T < 950$ K). Carbon monoxide had little impact on methane ignition delay at any of the conditions studied.
2. A fast sampling system and GC analysis were used to quantify the products of CH4 rich combustion. The results indicated a molar ratio of hydrogen to carbon monoxide of ~1.0, was produced which agreed well with predictions using AVL-Boost and equilibrium calculations. The yields of H_2 and CO mole fractions were approximately linear with increasing equivalence ratio, ranging from ~2% at $\phi = 1.1$ to ~10% at $\phi = 1.5$.
3. A D-EGR engine model was developed using AVL_BOOST software. Based on the simulation results, $CH_4/H_2/CO/CO_2/N_2$ mixtures were identified to represent the compositions of the stoichiometric and D-EGR cylinders. For the stoichiometric cylinder mixtures, the combustion duration decreased as equivalence ratio increased compared with $\phi = 1.0$ mixtures. For $\phi = 1.4$, the combustion duration decreased by about 25%. Conversely, combustion duration in the D-EGR cylinder increased with increasing equivalence ratio.
4. Apparent flame speeds were measured based on the combustion images acquired using high-speed imaging. Faster flame speeds were consistently observed for the stoichiometric cylinder mixtures as the equivalence ratio of the D-EGR cylinder increased, indicating H2 generated in the D-EGR enhanced combustion. However, although higher equivalence ratios in the D-EGR cylinder generated more H2, the flame speed in the D-EGR cylinder decreased with increasing equivalence ratio.

The results of the study show the trade-off between enhancing the combustion in the stoichiometric cylinders via the products of the D-EGR cylinder, with weaker combustion as the equivalence ratio is increased in the D-EGR cylinder. Since the RCM is designed to suppress mixing and turbulence, the results do not include the effects of the high turbulence intensities found in engines. Higher turbulence intensity can enhance flame propagation in the D-EGR cylinder, and can be a mechanism to improve combustion performance at fuel rich conditions. The results of the current study provide a quantitative basis for designing initial D-EGR fueling strategies for natural gas. The experimental data also provide expectation of the sensitivity of system response to a range of mixture compositions at well-defined state conditions.

Acknowledgment

This work is sponsored by the Project of National Natural Science Foundation of China under Grant no. 91541206 and the Project of State Key Laboratory of Automotive Safety and Energy under Grant no. ZZ2014-072.

Supplementary materials

Supplementary material associated with this article can be found, in the online version, at doi:10.1016/j.combustflame.2017.09.031.

References

[1] H.M. Cho, B. He, Spark ignition natural gas engines—a review, Energy Convers. Manag. 48 (2007) 608–618.
[2] A. Ibrahim, S. Bari, Optimization of a natural gas SI engine employing EGR strategy using a two-zone combustion model, Fuel 87 (2008) 1824–1834.
[3] R. Semin, A. Bakar, A technical review of compressed natural gas as an alternative fuel for internal combustion engines, Am. J. Eng. Appl. Sci. 1 (2008) 302–311.
[4] T. Korakianitis, A.M. Namasivayam, R.J. Crookes, Natural-gas fueled spark-ignition (SI) and compression-ignition (CI) engine performance and emissions, Prog. Energy Combust. 37 (2011) 89–112.
[5] A.K. Sen, S.K. Ash, B. Huang, Z. Huang, Effect of exhaust gas recirculation on the cycle-to-cycle variations in a natural gas spark ignition engine, Appl. Thermal Eng. 31 (2011) 2247–2253.
[6] T. Gatts, S. Liu, C. Liew, B. Ralston, C. Bell, H. Li, An experimental investigation of incomplete combustion of gaseous fuels of a heavy-duty diesel engine supplemented with hydrogen and natural gas, Int. J. Hydrogen Energy 37 (2012) 7848–7859.
[7] F. Moreno, M. Muñoz, J. Arroyo, O. Magén, C. Monné, I. Suelves, Efficiency and emissions in a vehicle spark ignition engine fueled with hydrogen and methane blends, Int. J. Hydrogen Energy 37 (2012) 11495–11503.
[8] P.M. Diéguez, J.C. Urroz, S. Marcelino-Sádaba, A. Pérez-Ezcurdia, M. Benito-Amurrio, D. Sáinz, L.M. Gandía, Experimental study of the performance and emission characteristics of an adapted commercial four-cylinder spark ignition engine running on hydrogen–methane mixtures, Appl. Energy 113 (2014) 1068–1076.
[9] L. Selle, T. Poinsot, B. Ferret, Experimental and numerical study of the accuracy of flame-speed measurements for methane/air combustion in a slot burner, Combust. Flame 158 (2011) 146–154.
[10] J. Beeckmann, L. Cai, H. Pitsch, Experimental investigation of the laminar burning velocities of methanol, ethanol, n-propanol, and n-butanol at high pressure, Fuel 117 (2014) 340–350.
[11] Y. Wu, V. Modica, B. Rossow, F. Grisch, Effects of pressure and preheating temperature on the laminar flame speed of methane/air and acetone/air mixtures, Fuel 185 (2016) 577–588.
[12] W. Lowry, J. d. Vries, M. Krejc, E. Petersen, Z. Serinyel, W. Metcalfe, H. Curran, G. Bourque, Laminar flame speed measurements and modeling of pure alkanes and alkane blends at elevated pressures, J. Eng. Gas Turbines Power 133 (2011) 091501.
[13] E. Varea, V. Modica, A. Vandel, B. Renou, Measurement of laminar burning velocity and Markstein length relative to fresh gases using a new postprocessing procedure: application to laminar spherical flames for methane, ethanol and isooctane/air mixtures, Combust. Flame 159 (2012) 577–590.
[14] A. Mze Ahmed, S. Mancarella, P. Desgroux, L. Gasnot, J.F. Pauwels, A. El Bakali, Experimental and numerical study on rich methane/hydrogen/air laminar premixed flames at atmospheric pressure: effect of hydrogen addition to fuel on soot gaseous precursors, Int. J. Hydrogen Energy 41 (2016) 6929–6942.
[15] Z. Chen, P. Dai, S. Chen, A model for the laminar flame speed of binary fuel blends and its application to methane/hydrogen mixtures, Int. J. Hydrogen Energy 37 (2012) 10390–10396.
[16] F. Halter, C. Chauveau, N. Djebaïli-Chaumeix, I. Gökalp, Characterization of the effects of pressure and hydrogen concentration on laminar burning velocities of methane–hydrogen–air mixtures, Proc. Combust. Inst. 30 (2005) 201–208.
[17] E. Hu, Z. Huang, J. He, C. Jin, J. Zheng, Experimental and numerical study on laminar burning characteristics of premixed methane–hydrogen–air flames, Int. J. Hydrogen Energy 34 (2009) 4876–4888.
[18] J. Liu, X. Zhang, T. Wang, X. Hou, J. Zhang, S. Zheng, Numerical study of the chemical, thermal and diffusion effects of H_2 and CO addition on the laminar flame speeds of methane–air mixture, Int. J. Hydrogen Energy 40 (2015) 8475–8483.
[19] S. Bougrine, S. Richard, A. Nicolle, D. Veynante, Numerical study of laminar flame properties of diluted methane–hydrogen–air flames at high pressure and temperature using detailed chemistry, Int. J. Hydrogen Energy 36 (2011) 12035–12047.
[20] M. Yu, K. Zheng, L. Zheng, T. Chu, P. Guo, Effects of hydrogen addition on propagation characteristics of premixed methane/air flames, J. Loss Prev. Proc. Ind. 34 (2015) 1–9.
[21] C. White, R. Steeper, A. Lutz, The hydrogen-fueled internal combustion engine: a technical review, Int. J. Hydrogen Energy 31 (2006) 1292–1305.
[22] P. Dimopoulos, C. Bach, P. Soltic, K. Boulouchos, Hydrogen–natural gas blends fuelling passenger car engines: combustion, emissions and well-to-wheels assessment, Int. J. Hydrogen Energy 33 (2008) 7224–7236.
[23] P. Dimopoulos, C. Rechsteiner, P. Soltic, C. Laemmle, K. Boulouchos, Increase of passenger car engine efficiency with low engine-out emissions using hydrogen–natural gas mixtures: a thermodynamic analysis, Int. J. Hydrogen Energy 32 (2007) 3073–3083.
[24] E. Hu, Z. Huang, B. Liu, J. Zheng, X. Gu, Experimental study on combustion characteristics of a spark-ignition engine fueled with natural gas–hydrogen blends combining with EGR, Int. J. Hydrogen Energy 34 (2009) 1035–1044.
[25] T. Alger, B. Mangold, Dedicated EGR: a new concept in high efficiency engines, SAE 2009-01-0694.
[26] C. Chadwell, T. Alger, J. Zuehl, R. Gukelberger, A demonstration of dedicated EGR on a 2.0 L GDI engine, SAE Int. J. Eng. 7 (2014) 434–447.
[27] S. Lee, K. Ozaki, N. Iida, T. Sako, A Potentiality of Dedicated EGR in SI Engines Fueled by Natural Gas for Improving Thermal Efficiency and Reducing NOx Emission, SAE Int. J. Eng. 8 (2015) 238–249.
[28] C.J. Goy, A.J. Moran, G.O. Thomas, Autoignition characteristics of gaseous fuels at representative gas turbine conditions, IGTI ASME 2001-GT-0051.
[29] E.L. Petersen, D.F. Davidson, R.K. Hanson, Kinetics modeling of shock-induced ignition in low-dilution CH_4–O_2 mixtures at high pressures and intermediate temperatures, Combust. Flame 117 (1999) 272–290.
[30] N. Donohoe, K.A. Heufer, C.J. Aul, E.L. Petersen, G. Bourque, R. Gordon, H.J. Curran, Influence of steam dilution on the ignition of hydrogen, syngas and natural gas blends at elevated pressures, Combust. Flame 162 (2015) 1126–1135.
[31] S. Gersen, N. Anikin, A. Mokhov, H. Levinsky, Ignition properties of methane/hydrogen mixtures in a rapid compression machine, Int. J. Hydrogen Energy 33 (2008) 1957–1964.
[32] S. Gersen, H. Darmeveil, H. Levinsky, The effects of CO addition on the autoignition of H_2, CH_4 and CH_4/H_2 fuels at high pressure in an RCM, Combust. Flame 159 (2012) 3472–3475.
[33] Y. Yu, G. Vanhove, J.F. Griffiths, S. De Ferrières, J.F. Pauwels, Influence of EGR and syngas components on the autoignition of natural gas in a rapid compression machine: a detailed experimental study, Energy Fuel. 27 (2013) 3988–3996.
[34] U. Burke, K.P. Somers, P. O'Toole, C.M. Zinner, N. Marquet, G. Bourque, E.L. Petersen, W.K. Metcalfe, Z. Serinyel, H.J. Curran, An ignition delay and kinetic modeling study of methane, dimethyl ether, and their mixtures at high pressures, Combust. Flame 162 (2015) 315–330.
[35] L. Brett, J. Macnamara, P. Musch, J.M. Simme, Simulation of methane autoignition in a rapid compression machine with creviced pistons, Combust. Flame 124 (2001) 326–329.
[36] D Healy, H.J. Curran, J.M. Simmie, D.M. Kalitan, C.M. Zinner, A.B. Barrett, E.L. Petersen, G Bourque, Methane/ethane/propane mixture oxidation at high pressures and at high, intermediate and low temperatures, Combust. Flame 155 (2008) 441–448.
[37] S. Heyne, A. Roubaud, M. Ribaucour, G. Vanhove, R. Minetti, D. Favrat, Development of a natural gas reaction mechanism for engine simulations based on rapid compression machine experiments using a multi-objective optimisation strategy, Fuel 87 (2008) 3046–3054.
[38] J. Huang, P.G. Hill, W.K. Bushe, S.R. Munshi, Shock-tube study of methane ignition under engine-relevant conditions: experiments and modeling, Combust. Flame 136 (2004) 25–42.
[39] E.L. Petersen, D.M. Kalitan, S. Simmons, G. Bourque, H.J. Curran, J.M. Simmie, Methane/propane oxidation at high pressures: experimental and detailed chemical kinetic modeling, Proc. Combust. Inst. 31 (2007) 447–454.
[40] M. Frenklach, H. Wang, M. Goldenberg, G.P. Smith, D.M. Golden, C.T. Bowman, R.K. Hanson, W.C. Gardiner, V Lissianski, GRI-Mech—an optimized detailed chemical reaction mechanism for methane combustion, The Gas Research Institute, November 1, 1995, Report No. GRI-95/0058.
[41] A. Demirbas, Methane gas hydrate, Spring-Veriag, London, 2010.
[42] Y. Li, C. Zhou, K.P. Somers, K. Zhang, H.J. Curran, The oxidation of 2-butene: a high pressure ignition delay, kinetic modeling study and reactivity comparison with isobutene and 1-butene, Proc. Combust. Inst. 36 (2017) 403–411.
[43] J. Huang, W.K. Bushe, P.G. Hill, S.R. Munshi, Experimental and kinetic study of shock initiated ignition in homogeneous methane–hydrogen–air mixtures at engine-relevant conditions, Int. J. Chem. Kinet. 38 (2006) 221–233.
[44] Y. Zhang, Z. Huang, L. Wei, J. Zhang, C.K. Law, Experimental and modeling study on ignition delays of lean mixtures of methane, hydrogen, oxygen, and argon at elevated pressures, Combust. Flame 159 (2012) 918–931.
[45] Y. Zhang, X. Jiang, L. Wei, J. Zhang, C. Tang, Z. Huang, Experimental and modeling study on auto-ignition characteristics of methane/hydrogen blends under engine relevant pressure, Int. J. Hydrogen Energy 37 (2012) 19168–19176.
[46] N. Donohoe, A. Heufer, W.K. Metcalfe, H.J. Curran, M.L. Davis, O. Mathieu, D. Plichta, A. Morones, E.L. Petersen, F. Güthe, Ignition delay times, laminar flame speeds, and mechanism validation for natural gas/hydrogen blends at elevated pressures, Combust. Flame 161 (2014) 1432–1443.
[47] A. Mariani, M.V. Prati, A. Unich, B. Morrone, Combustion analysis of a spark ignition i. c. engine fuelled alternatively with natural gas and hydrogen-natural gas blends, Int. J. Hydrogen Energy 38 (2013) 1616–1623.
[48] F. Ma, Y. Wang, H. Liu, Y. Li, J. Wang, S. Zhao, Experimental study on thermal efficiency and emission characteristics of a lean burn hydrogen enriched natural gas engine, Int. J. Hydrogen Energy 32 (2007) 5067–5075.
[49] M. Bysveen, Engine characteristics of emissions and performance using mixtures of natural gas and hydrogen, Energy 32 (2007) 482–489.
[50] J. Wang, Z. Huang, Y. Fang, B. Liu, K. Zeng, H. Miao, D. Jiang, Combustion behaviors of a direct-injection engine operating on various fractions of natural gas–hydrogen blends, Int. J. Hydrogen Energy 32 (2007) 3555–3564.
[51] I. Saanum, M. Bysveen, P. Tunestål, B. Johansson, Lean burn versus stoichiometric operation with EGR and 3-way catalyst of an engine fueled with natural gas and hydrogen enriched natural gas, SAE 2007-01-0015.

[52] H. Di, X. He, P. Zhang, Z. Wang, M.S. Wooldridge, C.K. Law, C. Wang, S. Shuai, J. Wang, Effects of buffer gas composition on low temperature ignition of iso-octane and n-heptane, Combust. Flame 161 (2014) 2531–2538.
[53] Z. Wang, Y. Qi, X. He, J. Wang, S. Shuai, C.K. Law, Analysis of pre-ignition to super-knock: hotspot-induced deflagration to detonation, Fuel 144 (2015) 222–227.
[54] W. Ji, P. Zhang, T. He, Z. Wang, L. Tao, X. He, C.K. Law, Intermediate species measurement during iso-butanol auto-ignition, Combust. Flame 162 (2015) 3541–3553.
[55] CHEMKIN release 10131, Reaction Design, San Diego (2013).
[56] X. He, S.M. Walton, B.T. Zigler, M.S. Wooldridge, A. Atreya, Experimental investigation of the intermediates of isooctane during ignition, Int. J. Chem. Kinet. 39 (2007) 498–517.
[57] A.A. Mira, M.M. Wanib, Computational analysis of performance and emissions of a compression ignition engine under various air induction methods, Int. J. Therm. Environ. Eng. 9 (2015) 47–52.
[58] J.B. Heywood, Internal combustion engine fundamentals, Mcgraw-hill, New York, 1988.